Electronic Spectrum of Trigonal Selenium

ROLF SANDROCK*
The James Franck Institute, The University of Chicago, Chicago, Illinois 60637
(Received 22 December 1967)

From empirical form factors for cubic ZnSe, a pseudopotential is derived for elemental selenium. With some minor adjustment to obtain the direct experimental gap, this pseudopotential is used to calculate energy bands along all symmetry axes of the Brillouin zone. Based on a coarse regular point mesh and quadratic interpolation, the imaginary part of the dielectric function is calculated in the random-phase approximation. Fairly good agreement is obtained with the measured optical spectrum, and some of the observed peaks are identified. It is found that the spectrum is determined not only by the joint density of states but also very strongly by variations in k space of the oscillator strengths. The real part of the dielectric function and the reflectivity spectrum have also been calculated for polarizations parallel and perpendicular to the trigonal axis.

I. INTRODUCTION

IN spite of its great practical importance, selenium is probably less well understood with regard to its electronic structure than any other elemental semiconductor. One reason for this is its peculiar, highly anisotropic crystal structure[1] that makes the analysis complicated and the usual approximations doubtful. First-principles calculations have been performed following the tight-binding[1,2] and Korringa-Kohn-Rostoker[3] (KKR) formalisms. The former of these, while not inappropriate in principle, included only one symmetry axis. The latter method assumes a muffin-tin-type potential which is hard to justify for the present case. No pseudopotential band structure has yet been published for selenium, though such calculations have been done for the closely related element tellurium.[4,5]

Because of the limited theoretical results available, optical experiments[6–8] have so far been interpreted in terms of band-to-band transitions at symmetry points. But the experience with cubic semiconductors[9,10] strongly suggests that this may not be adequate in many cases. Rather, one should expect that any part of the Brillouin zone may be responsible for a certain peak in the reflectivity spectrum. Therefore it was felt that this calculation should (a) include all the symmetry lines and (b) cover the entire zone at least in a crude mesh.

An interesting feature of the optical spectrum of selenium is its pronounced polarization dependence. This facilitates comparison of theoretical contributions with the experimental spectrum.

II. SYMMETRY

The crystal structure of selenium and its group-theoretical implications have been dealt with by several authors (e.g., Refs. 1 and 3). For further reference, Fig. 1 shows the Brillouin zone with all the points and axes that occur in our calculation. Not all of them are truly symmetry points, since the selenium point group does not contain all elements of the full hexagonal group. Only the axes Δ, P, Σ, and S (including the points Γ, A, K, H) have wave vector groups with elements other than the identity. Strictly speaking, neighboring corners H and H' are not equivalent; however, their term schemes are degenerate by time reversal, so we need not distinguish between them.

The wedge $AMHAMH$ is the irreducible part of the Brillouin zone, i.e., the entire zone can be generated from it by applying the six point-group operations plus time-reversal symmetry, which effectively acts as an inversion. (There is no element to convert the upper half of the wedge into the lower one.) It is this irreducible wedge that has to be exhausted in the calculation of ϵ_2, the imaginary part of the dielectric function $\epsilon(\omega)$.

III. PSEUDOPOTENTIAL

The correct choice of a pseudopotential is crucial for our problem. Previous examples have shown that an *ad hoc* construction from atomic functions may be hazardous[4] and that the full strength of the pseudo-

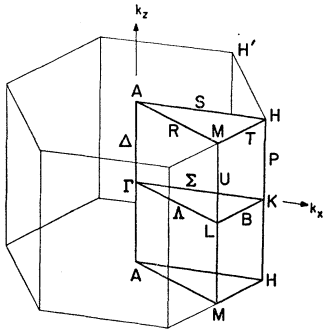

FIG. 1. Brillouin zone for selenium with irreducible wedge.

* On leave from the University of Marburg, Marburg, Germany.
[1] J. R. Reitz, Phys. Rev. **105**, 1233 (1957).
[2] D. J. Olechna and R. S. Knox, Phys. Rev. **140**, A986 (1965).
[3] J. Treusch and R. Sandrock, Phys. Status Solidi **16**, 487 (1966).
[4] R. E. Beissner, Phys. Rev. **145**, 479 (1966).
[5] M. Picard and M. Hulin, Phys. Status Solidi **23**, 563 (1967).
[6] J. Stuke and H. Keller, Phys. Status Solidi **7**, 189 (1964).
[7] E. Mohler, J. Stuke, and G. Zimmerer, Phys. Status Solidi **22**, K49 (1967).
[8] S. Tutihasi and I. Chen, Phys. Rev. **158**, 623 (1967).
[9] D. Brust, Phys. Rev. **134**, 1337 (1964).
[10] E. O. Kane, Phys. Rev. **146**, 558 (1966).

potential approach is observed only if the form factors are determined from experiment.[9,11] Although there are optical data available for selenium,[6–8] these cannot be used, since their interpretation is doubtful; in fact, this is just what this paper is to elucidate. However, Cohen and Bergstresser[11] have given pseudopotential form factors for a number of zincblende-type semiconductors, including ZnSe.

This information can now be exploited to calculate energy bands for other crystals involving the same constituents, as suggested by Phillips.[12] Basically, no further adjustment should be necessary with this approach.

Thus our atomic form factors $v_{\mathrm{Se}}(q)$ were obtained from

$$v_{\mathrm{Se}}(q)=c(v^s(q)-v^a(q)), \tag{1}$$

where v^s and v^a are the symmetric and antisymmetric parts, respectively, of Cohen and Bergstresser's[11] form factors for ZnSe. The constant $c=\frac{3}{2}\Omega_{\mathrm{ZnSe}}/\Omega_{\mathrm{Se}}$ accounts for the different unit cell volumes and numbers of atoms per unit cell in the selenium and ZnSe structures. Multiplying $v_{\mathrm{Se}}(q)$ by the appropriate structure factor

$$s_{\mathrm{Se}}(\mathbf{q})=\tfrac{1}{3}\sum_{i=1}^{3} e^{i\mathbf{q}\cdot\mathbf{t}i}, \tag{2}$$

where $\mathbf{t}_i$ denotes the location of the ith atom in the cell, we get the pseudopotential coefficients for trigonal selenium.

Of course, this procedure requires interpolation between Cohen and Bergstresser's $v(q)$ and even extrapolation beyond their q range. The first reciprocal lattice vectors for selenium are shorter than the (1,1,1) vector for ZnSe. But this extrapolation ambiguity does not affect the more relevant bands to within 0.01 Ry. When extrapolating $v(q)$ towards large q, the model potential of Animalu and Heine[13] was followed as a guideline (Fig. 2).

Using the pseudopotential just described, energy bands were calculated along the P axis, since this is the region where, according to earlier calculations,[3] the energy gap was expected to occur (Fig. 3, left-hand side). We find a direct gap of 1.4 eV, compared with an experimental value of $E_G=2.0$ eV.[8] The agreement is considered satisfactory in view of the drastic difference between the crystal structures of ZnSe and Se.

Moreover, the discrepancy can be removed by a moderate adjustment of the form factors (Fig. 2). Since there are so many different reciprocal lattice vectors involved, there is no point in fitting just one or a few of them to obtain the experimental gap. Instead, this was achieved by slightly raising the entire form-factor curve for $q>k_F\approx 1r_B^{-1}$. (Note that

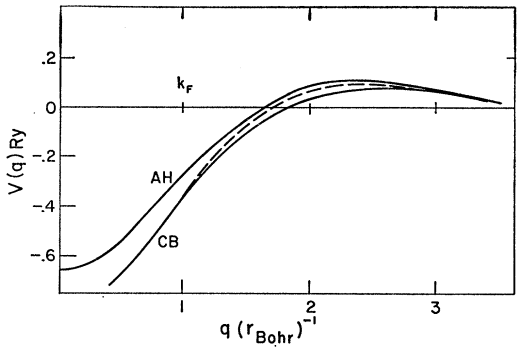

FIG. 2. Pseudopotential form factors for selenium. CB—derived from Cohen and Bergstresser (Ref. 11); AH—model potential after Animalu and Heine (Ref. 13); dashed line—adjusted pseudopotential.

the Cohen and Bergstresser form factors are only accurate to within 0.01 Ry.) The adjusted pseudopotential lies between the ones of Cohen and Bergstresser[11] and of Animalu and Heine,[13] indicating that the dielectric screening seems to be somewhat more metallic in elemental selenium than it is in ZnSe.

The result of this somewhat artificial change is shown in Fig. 3, right-hand side. Except for the desired broadening of the gap, it seems to affect merely the higher conduction bands. It is this adjusted pseudopotential that was used in the further calculations.

The pseudopotential employed in either form is a local one. It was felt that nonlocality should have a negligible effect in the present case where both valence and conduction states have predominantly p character (except for the higher conduction bands which essentially correspond to atomic $5s$ states[2]). Also, spin-orbit interaction has not been taken into account. Splittings due to spin are expected to be small for selenium, though they may be important for tellurium.

IV. OPTICAL SPECTRUM

The optical properties of a crystal are described by its complex dielectric function $\epsilon(\omega)$, the imaginary part

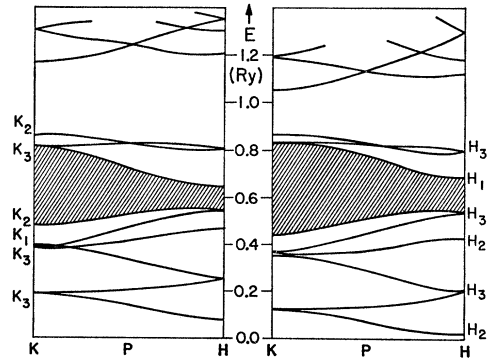

FIG. 3. Calculated energy bands along the P axis. Left—using the CB pseudopotential of Fig. 2. Right—using the adjusted pseudopotential.

[11] M. L. Cohen and T. K. Bergstresser, Phys. Rev. **141**, 789 (1966).
[12] J. C. Phillips, J. Phys. Soc. Japan Suppl. **21**, 3 (1966).
[13] A. O. E. Animalu and V. Heine, Phil. Mag. **12**, 1249 (1965); A. O. E. Animalu, Technical Report No. 4, 1965, Solid State Group, Cavendish Laboratory, Cambridge, England (unpublished).

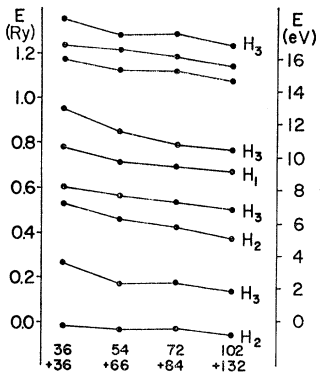

FIG. 4. Convergence behavior of eigenvalues at point H. The two numbers below each term ladder are the numbers of plane waves included exactly and approximately.

of which is given by[9]

$$\epsilon_2^{(jj)}(\omega)=\frac{4\pi^2e^2\hbar}{m^2\omega^2}\sum_{n,s}\int_{\text{B.Z.}}\frac{2}{(2\pi)^3}\delta[\omega_{ns}(\mathbf{k})-\omega]\times|M_{n,s}^{(j)}(\mathbf{k})|^2d^3k. \quad (3)$$

Here the subscripts n and s denote filled and unfilled bands, respectively, $\omega_{ns}(\mathbf{k})=[E_s(\mathbf{k})-E_n(\mathbf{k})]/\hbar$, and the interband oscillator strength is

$$M_{n,s}^{(j)}(\mathbf{k})=\frac{1}{i\Omega}\int\psi_{\mathbf{k}n}^*\frac{\partial}{\partial x_j}\psi_{\mathbf{k}s}d^3r \quad (4)$$

integrated over the unit cell of volume Ω. The superscripts jj are the indices of the dielectric tensor. In the crystal coordinate system there are no off-diagonal elements, and since selenium is a uniaxial crystal, we have only two different diagonal components, $||$ and $\perp$, with respect to the c axis.

In the cubic semiconductors, it is a fair approximation[9] to assume $M_{n,s}(\mathbf{k})$ to be independent of $\mathbf{k}$. This is of course not possible in our case, because selection rules will require either $M_{n,s}^{||}$ or $M_{n,s}^{\perp}$ to vanish at certain symmetry points.[3] To calculate $M_{n,s}^{||}(\mathbf{k})$, $M_{n,s}^{\perp}(\mathbf{k})$, the pseudopotential wave functions were used in Eq. (4), i.e., only the smooth parts ϕ of ψ. This procedure gives correct oscillator strengths[14] to within 20% for light elements like Si. For heavier elements (such as Ge or Se, which contain d core electrons), the oscillator strengths obtained from ϕ may be less accurate, as it has been observed in the case of SnTe.[15]

Equation (3) describes the dielectric function within the random-phase approximation. Exciton contributions are therefore not contained in our formalism. Likewise, indirect transitions are excluded from the calculation.

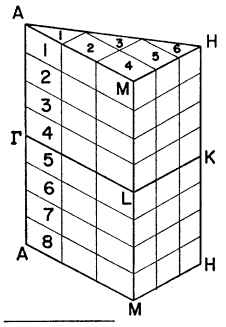

FIG. 5. The irreducible wedge divided into 48 subzones.

[14] L. Kleinman and J. C. Phillips, Phys. Rev. **118**, 1153 (1960).

V. COMPUTATIONAL DETAILS

A. Energy Bands

Preliminary studies[16] made obvious that a much larger set of plane waves has to be included in a pseudopotential calculation of selenium than had been necessary for cubic semiconductors.[9] Hence the size of the secular determinants causes problems with regard to both computer time and storage capacity. Although their dimension may be cut down by a factor of 3 on the axes Δ and P and by a factor of 2 on Σ and S by use of symmetry arguments, this is not possible at any other point.

As an example of the convergence behavior, the energy levels at H are plotted in Fig. 4 for four different stages. The numbers specified below are the number of plane waves treated exactly (top number) and of those included approximately by Löwdin perturbation[9] (bottom number). The final choice for the band calculations discussed below [Figs. 6(a)–(c)] corresponds to convergence stage 3 of Fig. 4, i.e., using a fixed cutoff energy of 55 eV for the plane waves treated exactly, their number varying between 70 and 80 depending on $\mathbf{k}$. For the ϵ_2 calculation, the convergence at the mesh points was that of stage 2, i.e., between 54 and 62 plane waves at 48-eV cutoff energy. In neither case is the absolute convergence of the levels perfect. However, including more plane waves will lower them rather uniformly. Moreover, if we look at energy differences instead of absolute levels, the general trend for most interband energies at most of the points investigated is to decrease slightly with increasing number of plane waves. From this we estimate the error in the transition energies to fall between 0 and +0.5 eV.

B. Imaginary Part of Dielectric Function

In order to compute the integral (3) numerically, we approximate it by a sum over a finite number N of k points[9]:

$$\epsilon_2^{(j)}(\omega)=\frac{4\pi^2e^2\hbar}{m^2\omega^2}\frac{2}{(2\pi)^3}\frac{V_{\text{BZ}}}{\Delta\omega\cdot N}\sum_{n,s}\sum_{\mathbf{k}}\delta^{\Delta\omega}(\omega_{ns}(\mathbf{k})-\omega)\times|M_{n,s}^{(j)}(\mathbf{k})|^2. \quad (5)$$

[15] P. J. Lin, W. Saslow, and M. L. Cohen, Solid State Commun. **5**, 893 (1967).

[16] R. Sandrock, in *Proceedings of the First Symposium on the Physics of Se and Te, Montreal, 1967* (Pergamon Press, Inc., New York, to be published).

V_{BZ} is the volume of the Brillouin zone, $\delta^{\Delta\omega}(\omega-\omega')=1$ if $|\omega-\omega'|<\frac{1}{2}\Delta\omega$ and $=0$ otherwise. This will give us ϵ_2 as a histogram function, defined at discrete points. These are separated by intervals $\hbar\Delta\omega=1/300$ Ry.

This sampling procedure requires a large number of points, many more than we can afford to calculate by actually solving the pseudopotential determinants. Instead, eigenvalues and eigenvectors were obtained only at the centers of 48 subzones into which the irreducible wedge of Fig. 1 had been divided (Fig. 5). Within each subzone, the interband energies $E_{ns}=\hbar\omega_{ns}$ were interpolated using a quadratic expansion around the center $\mathbf{k}_0$:

$$E_{ns}(\mathbf{k})=E_{ns}(\mathbf{k}_0)+\sum_i(\mathbf{k}_i-\mathbf{k}_{0i})p_i+\sum_{ij}(\mathbf{k}_i-\mathbf{k}_{0i})q_{ij}(\mathbf{k}_j-\mathbf{k}_{0j}), \quad (6)$$

where the nine coefficients p_i, q_{ij}, $i\geqslant j$ were determined using the condition that the transition energies at neighboring mesh points should fulfill Eq. (6). For the oscillator strengths $|M_{ns}^{\parallel,\perp}(\mathbf{k})|^2$ a linear expansion was applied. The restriction to a 48-point mesh can be justified by the flat bands of selenium. In this case the quadratic interpolation should give a reasonable accuracy. Besides, it is so fast on a modern computer that the $\mathbf{k}$ sum in (5) can easily be extended over a large number of points. Two figures may be illustrative in this context: While it took 140 min on an IBM 360/75 computer to solve the secular equation for 48 mesh points, the interpolation for 50 000 random points was done in 18 min. With this number, the average histogram scatter is only 1 or 2%. In fact, the accuracy and resolution of our sampling technique is such that it will introduce virtually no error in addition to the ones inherent in our pseudopotential calculation and in the quadratic interpolation.

Six valence and six conduction bands were included in the n-s sum in Eq. (5). This gave contributions up to 12 eV. In order to get maximum information about the origin of the optical structure, ϵ_2 contributions were discriminated according to which band pairs they came from (results are shown in Figs. 9 and 10). Furthermore, to trace localized contributions, an H neighborhood was defined by cutting out spheres of radius $\pi/2c$ around the H points. Similarly, a Δ neighborhood (including Γ and A) was defined to be the cylinder of radius $\pi/3a$ around the Δ axis. Either neighborhood contains about one-eighth of the Brillouin-zone volume. Finally, the zone was divided into halves, $0<|k_z|<\pi/2c$ and $\pi/2c<|k_z|<\pi/c$. The contributions from all these k space regions were added up separately (results in Fig. 8).

VI. RESULTS

A. Energy Bands

In Fig. 6, the pseudopotential energy bands are plotted. Figures 6(a) and (b) show their behavior in the

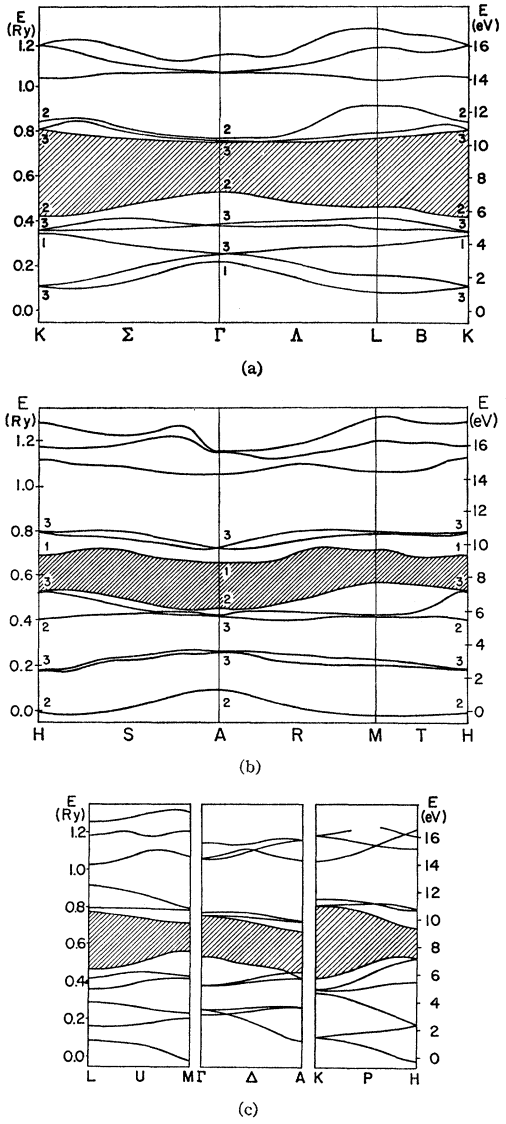

FIG. 6. Calculated energy bands, using the adjusted pseudopotential of Fig. 2. (a) Points and axes with $k_z=0$. (b) Points and axes with $k_z=\pi/c$. (c) Connecting vertical axes (numbers denote representations).

planes $k_z=0$ and $k_z=\pi/c$, respectively. A striking result is that quite generally the semiconductor gap is much broader in the first plane than in the second. From Fig. 6(c), where the vertical axes are drawn, we see that the decrease in gap width from L to M is quite similar to the behavior between K and H.

Point M has no special symmetry in the selenium structure and had therefore not been considered previously. We find, however, that the gap at M is approximately as small as at H —even slightly smaller, according to Table I. The smallest separation between valence and conduction band is confirmed to occur in the neighborhood of H as in earlier calculations,[3] but it seems now to be located on the T axis between H and

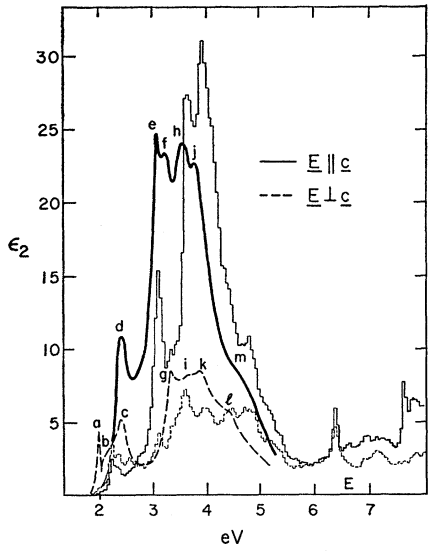

FIG. 7. Experimental ϵ_2 curves (Ref. 8) and calculated histograms for $\mathbf{E}\|\mathbf{c}$ (solid) and $\mathbf{E}\perp\mathbf{c}$ (dashed).

M. Of course, there is strictly no reason why it could not be a yet more general point. But this may not be likely, because the gradient of energy must be zero perpendicular to the T axis. Midway between H and M, the H selection rules are still approximately valid: In fact, the perpendicular oscillator strength was found to be 50 times as large as for parallel polarization.

Comparing our energy bands with the results of earlier KKR calculations,[3] we find qualitative similarities. However, all bandwidths and interband energy differences have nearly doubled. It is not surprising that the muffin-tin approximation thus turns out to make the bands too flat, since the muffin-tin spheres fill only 24% of the unit cell for selenium.

B. Oscillator Strengths

Figure 7 shows the calculated ϵ_2 spectrum for polarization parallel and perpendicular to the trigonal c axis, together with the experimental curves by Tutihasi and Chen.[8] The most surprising fact is the excellent agreement in the over-all height of the spectra, obtained without any adjustment. It indicates that on the average our pseudo-wave-function oscillator strengths might be better than anticipated. A possible explanation could be that the oscillator strengths are determined to a large extent by the built-in symmetry; at least this should fix the ratio between the parallel and perpendicular components. Since the oscillator strengths will play an important role in the interpretation of the curves, they are compiled in Table II for all 48 mesh points and three of the more interesting transitions (out of 36 considered in the calculations). The numbers m, n correspond to the vertical and horizontal numbering of the mesh cells in Fig. 5. Hence $(m,n)=(1,1)$ is the cell near point A, (1,6) is near H, (4,1) is near Γ, and (4,6) is near K, with the selection rules[3] for these points being obeyed approximately in the corresponding cells.

From Table II we see that the oscillator strengths vary quite rapidly between different points of the Brillouin zone. This has to be taken into account when assignments are to be made as to the origin of certain structures in the optical spectrum. In blocks a and c of Table II, the oscillator strength seems to jump discontinuously between cells (1,1) and (1,2). But this is obviously caused by the crossing of bands along the Δ axis; the parallel transition is allowed for the top valence band at A but forbidden for the second valence band which becomes first along Δ.

VII. DISCUSSION OF THE ε_2 SPECTRUM

A. General

We are now in a position to compare the calculated results with the measurements.[6–8] It should be kept in mind, though, that the experimental ϵ_2 curves[8] in Fig. 7 have been obtained by Kramers-Kronig analysis from reflectivity measurements which were limited to energies below 6 eV. Since more recent ultraviolet reflectivity data[7] revealed unexpected structure at higher energies, the experimental ϵ_2 curves may have to be slightly modified. From our theoretical ϵ_2 histogram we have calculated backwards to obtain ϵ_1 and the reflectance R. This will be discussed in Sec. VIII.

One possible interpretation of Fig. 7 is to assume that the calculated energies are correct and that the transition matrix elements are off by a factor of up to 3. This view is favored by the general argument that variational methods tend to give more accurate results for the eigenvalues than for the eigenfunctions; it is also supported by the experience of previous ϵ_2 calcula-

TABLE I. Eigenvalues in eV for nine valence bands and six conduction bands at symmetry points. The forbidden gap is between the sixth and seventh rows. In case of degeneracy, both degenerate levels have been listed.

Γ	L	K	A	M	H
15.6	17.0	16.2	15.8	17.7	17.4
14.4	16.0	16.2	15.8	16.4	16.0
14.4	13.9	14.3	14.4	14.5	15.2
10.3	12.3	11.4	9.9	10.8	10.7
10.2	10.8	11.0	9.9	10.6	10.7
10.2	10.5	11.0	9.0	9.6	9.3
7.2	6.3	5.7	6.2	7.7	7.2
5.1	5.6	4.9	5.8	5.8	7.2
5.1	4.7	4.9	5.8	5.7	5.8
3.4	3.9	4.6	3.6	3.1	2.6
3.4	2.2	1.5	3.6	2.7	2.6
3.0	1.1	1.5	1.3	−0.4	−0.4
−3.8	−3.7	−3.8	−3.0	−0.6	−0.7
−3.8	−4.1	−3.8	−7.0	−6.9	−6.9
−8.3	−8.0	−8.2	−7.0	−7.0	−6.9

tions, e.g., of SnTe [15] and Cu [17] (the latter case being more complicated because of the d bands).

Let us recall, however, the conclusion drawn from our convergence studies (Fig. 4), namely, that our transition energies are probably too large, possibly by as much as 0.5 eV. If we correspondingly shift the peaks in our calculated histograms to the left, we get very close agreement with the experimental curves. In fact, we shall see in the following discussion that one-to-one assignments can be made for a number of peaks observed. Therefore we believe this interpretation of Fig. 7 to be more appropriate than the one mentioned before. Incidentally, the suggested energy shifts are of approximately the same magnitude as the ones encountered in Brust's calculation.[9]

B. Absorption Edge

We start our discussion at low energies; the labels on the experimental curves are taken from Tutihasi and Chen.[8] The first sharp spike a has already been identified[8,18] to be excitonic. This interpretation is confirmed by the fact that it does not show up in our calculation. Interband absorption starts with the bulge b which we identify with our first peak at 2.2 eV. Experimentally, this is found only with perpendicular polarization, while our calculation seems to claim a smaller parallel effect as well. But this is clearly spurious and due only to the crudeness of our model: We calculated the oscillator strengths at the mesh points, where the selection rules are not strictly fulfilled (cf. Table IIa). From Table IIa we further learn that the oscillator strengths for the edge transition in the region near H are all less than 0.1 Ry; this explains why ϵ_2 is rather small there. In fact, virtually all the contribution to ϵ_2 below 2.5 eV was found to come from the H neighborhood defined in Sec. VB (cf. Fig. 8, where $\epsilon_2^{\parallel}$ is plotted only in order to avoid confusion).

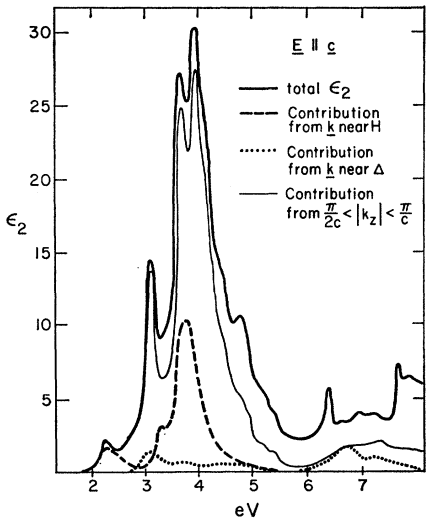

FIG. 8. Contributions to the calculated ϵ_2 spectrum from regions near H and Δ.

There has been some argument about whether the absorption edge in selenium is direct or indirect (see, e.g., Ref. 19). Our band model [Fig. 6(b)] strongly suggests that there will be indirect transitions (along the T axis and also between A and M) below the direct edge. On the other hand, as our ϵ_2 calculation proves, the gross features of the edge can be described in terms of direct transitions only. The good agreement between the calculated and measured curves shows that the indirect transitions are probably too weak to influence the reflectivity. However, they may well determine the fine structure below the edge and show up in the absorption coefficient.[19]

C. ε_2 at Intermediate Energies

Next to the absorption edge, Tutihasi and Chen[8] found a pronounced peak at 2.3 eV, labelled c in the

TABLE II. Interband momentum matrix elements $(2/m)M^2$ in Ry for three transitions, viz., (a) highest valence band VB_1 to lowest conduction band CB_6 (fundamental absorption edge), (b) third valence band VB_3 to lowest conduction band CB_6, and (c) highest valence band VB_1 to lowest subband CB_3 in the upper conduction band triplet. The oscillator strengths are given for each of the 48 mesh points which are characterized by their vertical and planar coordinate numbers m and n (*cf.* Fig. 5). In each box of the table, top and bottom numbers refer to parallel and perpendicular polarization, respectively.

IIa

$VB_1 \rightarrow CB_6$	$n=1$	2	3	4	5	6
$m=1$	0.117	0.084	0.087	0.044	0.052	0.038
	0.008	0.041	0.015	0.064	0.072	0.065
2	0.017	0.199	0.297	0.060	0.120	0.065
	0.009	0.032	0.033	0.045	0.075	0.076
3	0.012	0.155	0.013	0.046	0.115	0.013
	0.004	0.036	0.018	0.067	0.088	0.071
4	0.008	0.041	0.009	0.227	0.163	0.005
	0.006	0.042	0.030	0.059	0.066	0.025

IIb

$VB_3 \rightarrow CB_6$	$n=1$	2	3	4	5	6
$m=1$	0.016	0.199	0.222	0.268	0.536	0.686
	0.096	0.016	0.004	0.005	0.004	0.004
2	0.004	0.065	0.058	0.203	0.171	0.179
	0.099	0.032	0.009	0.041	0.018	0.006
3	0.024	0.010	0.104	0.055	0.015	0.013
	0.195	0.046	0.051	0.099	0.040	0.020
4	0.029	0.098	0.018	0.097	0.043	0.019
	0.075	0.090	0.056	0.067	0.054	0.056

IIc

$VB_1 \rightarrow CB_3$	$n=1$	2	3	4	5	6
$m=1$	0.819	0.083	0.070	0.013	0.020	0.032
	0.014	0.070	0.092	0.038	0.062	0.050
2	0.046	0.060	0.096	0.041	0.054	0.057
	0.003	0.108	0.058	0.057	0.032	0.004
3	0.078	0.398	0.074	0.173	0.209	0.305
	0.047	0.065	0.030	0.033	0.026	0.008
4	0.019	0.486	0.631	0.392	0.491	0.611
	0.088	0.021	0.025	0.021	0.019	0.010

[17] F. M. Mueller and J. C. Phillips, Phys. Rev. **157**, 600 (1967).

[18] W. Henrion, Phys. Status Solidi **22**, K33 (1967).

[19] G. G. Roberts, S. Tutihasi, and R. C. Keezer, Solid State Commun. **5**, 517 (1967).

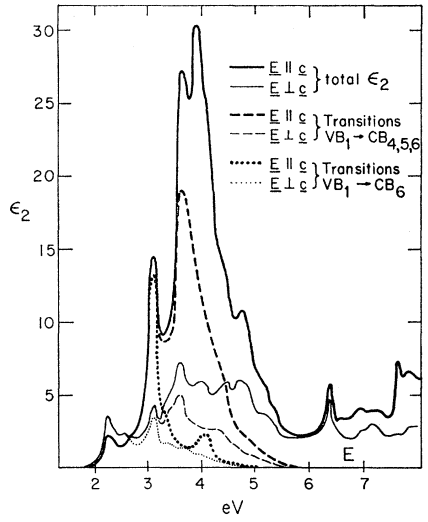

FIG. 9. Contributions to ϵ_2 involving the highest valence band VB_1.

perpendicular and *d* in the parallel spectrum. Taking into account the energy shift mentioned above, we identify this with our peak near 3 eV. Since it appears in either polarization, it is probably not connected with a single symmetry point. In fact, there is almost no contribution to it from the *H* neighborhood (Fig. 8), while the Δ neighborhood contributes only one-eighth, which is just its share in the total volume. The only safe conclusion about this peak can be drawn from Fig. 9, where ϵ_2 is decomposed according to the band pairs involved. This shows that not only the absorption edge but also the peaks *c*, *d* are caused entirely by transitions from the highest valence band to the lowest conduction band. From Table IIa we may then conjecture that their main contributions come from inner parts of the Brillouin zone near the mesh box labelled $m=2$, $n=3$.

The large structure between 3 and 4 eV (experimental) is clearly composed of several peaks. In fact, Fig. 9 shows that part of its left side is still due to transitions starting from the highest valence band, the final states now being in the second- or third-lowest conduction band. On the other hand, Fig. 8 reveals that there is also a large contribution coming from the region near *H*.

Considering the selection rules and the interband energy, this can only be due to the transition $VB_3 \rightarrow CB_6$ [third valence band to lowest (6th) conduction band]. In fact, Table IIb lists a very large oscillator strength near *H*. We believe, therefore, that a critical point at or near *H* gives rise to the observed peak *f* and that the exciton spike *e* (missing in the calculated spectrum) is associated with it.

Apparently the experimental peaks *h* and *j* have by accident coincided in our calculation, making the histogram peak below 4 eV narrower and slightly higher than it ought to be. They do not seem to be well localized. The same statement holds for the structure *g–i–k* in the perpendicular spectrum. The shoulder *m* shows up as a pronounced side-peak at 4.8 eV in our histogram, but no definite assignment can be made about its origin. According to Fig. 8, it is associated with the central part $|k_z| < (\pi/2c)$ of the Brillouin zone—unlike most of the low-energy structure which is to a large extent contributed by the outer regions near the hexagonal zone faces.

D. Higher Transitions

Up to $E=5.5$ eV, all contributions to ϵ_2 have exclusively been due to transitions from the upper valence band triplet to the lower conduction triplet. As may be seen from Fig. 10, these taper off between 5.5 and 6.5 eV. At the same time, transitions from the lower valence triplet begin to play a role. The result is a pronounced minimum near 6 eV for both polarizations. This proves the hypothesis of Mohler *et al.*,[7] who observed this deep minimum and explained it by a gap between the valence triplets. The *second absorption edge* at 6.2 eV in the calculated ϵ_2 curves is due to the lower triplet and resembles the fundamental edge.

At 7.6 eV there is another prominent peak in the parallel spectrum. Mohler *et al.* find a large peak in the reflectivity at 7.66 eV (cf. Fig. 12) with the same selection rule and attribute it to transitions from the lower valence triplet along the Δ axis. However, Fig. 8 does not indicate any considerable Δ contribution at that energy (though there is some at 6.7 eV). Instead, Fig. 10 shows that our 7.6-eV peak is caused by the sudden come-back of transitions from the top valence band, now going to the higher conduction band triplet. Looking at Fig. 6(a) and Table IIc, we find that this transition sets in over the entire $k_z \approx 0$ region at approximately the same energy and with large oscillator strength (except near Γ). This strong and steep *third absorption edge* adds to the contribution from the lower valence triplet which carries on until 10 eV. There is

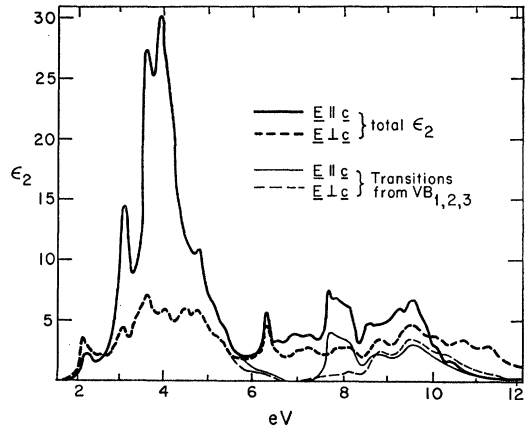

FIG. 10. Calculated ϵ_2 spectrum decomposed according to the initial states of the transitions contributing.

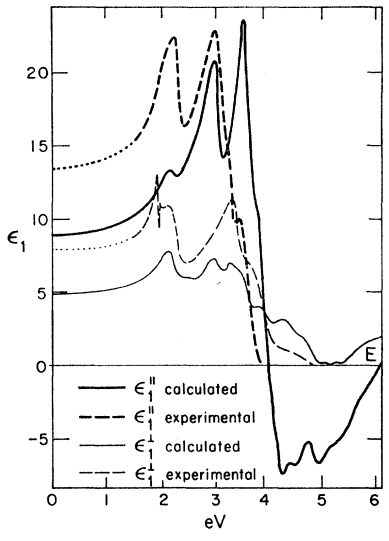

FIG. 11. Calculated and experimental ϵ_1 curves.

another peak for either polarization at 9.5 eV, which is just outside the range investigated experimentally; however, the rise towards it is clearly seen in the measurements[7] (Fig. 12).

VIII. REAL PART OF DIELECTRIC FUNCTION AND REFLECTIVITY SPECTRUM

From a theoretical point of view, the imaginary part $\epsilon_2(\omega)$ of the dielectric function offers the most natural way to describe the optical properties of a crystal. However, all our experimental information is based on reflectivity data (the absorption coefficient has been measured below the fundamental edge only[19]). Therefore we calculated the real part ϵ_1 of the dielectric function from our ϵ_2 histogram by means of the Kramers-Kronig dispersion relation (e.g., Ref. 20),

$$\epsilon_1(\omega)=1+\frac{2}{\pi}P\int_0^\infty \frac{\omega'\epsilon_2(\omega')d\omega'}{\omega'^2-\omega^2}. \quad (7)$$

With $\epsilon_1=n^2-\kappa^2$ and $\epsilon_2=2n\kappa$ the reflectivity R is then given by

$$R(\omega)=[(n-1)^2+\kappa^2]/[(n+1)^2+\kappa^2]. \quad (8)$$

The calculated ϵ_1 spectrum is drawn in Fig. 11, together with experimental curves[8] derived from reflectivity measurements. Besides an energy shift similar to the one found in Fig. 7, the absolute magnitude of ϵ_1 falls short of the empirical value. In particular, the static dielectric constants, although qualitatively correct in their polarization dependence, are too small, $\epsilon_1^{\parallel}(0)=8.9$ and $\epsilon_1^{\perp}(0)=4.9$, compared with 13.3 and 8, experimentally.[21] This can be understood for two reasons. First, the main contributions to our calculated ϵ_2 are at energies higher than to be expected experimentally (Fig. 7); according to Eq. (7), this will lower $\epsilon_1(0)$. In fact, we can resolve part of the discrepancy by shifting our ϵ_2 spectrum to lower energies. Applying a rigid shift by -0.5 eV, we obtain $\epsilon_1^{\parallel}(0)=10.0$ and $\epsilon_1^{\perp}(0)=5.4$; with a -0.7-eV shift, the numbers are 10.6 and 5.7, respectively. The remaining disagreement can be explained by the neglect of high-energy contributions to ϵ_2 beyond the sixth conduction band. This again has a decreasing effect on ϵ_1.

Figure 12 shows the reflectivity spectrum; the experimental curves have been taken from measurements by Stuke and co-workers.[7] The details of the structure have already been discussed in connection with the ϵ_2 spectrum. It should be pointed out that the sharp peaks (especially at high energies) are probably broadened by lifetime effects which have not been allowed for in our calculations.

IX. CONCLUSIONS

Perhaps the most noteworthy single feature of our results is the good over-all agreement between our calculations and experiment as to absolute magnitude for both parallel and perpendicular polarizations (Fig. 7). Then we have attempted to classify the various structures in the optical spectrum in terms of direct interband transitions located at specific points in the Brillouin zone. It turned out that only a few peaks (b, f) could be attributed to transitions that are localized in k space. The calculations were not accurate enough to perform a detailed critical-point analysis like the one Brust[9] did for Ge and Si. It appears that such an analysis is more difficult in the case of Se because of the reduced symmetry of the Brillouin zone, and the complexity and flatness of the bands. Moreover, it would probably be less fruitful, because we have found that the structure is caused in part by rapid variations in the interband oscillator strengths as much as by critical points in the joint density of states. In the past, interpretation of

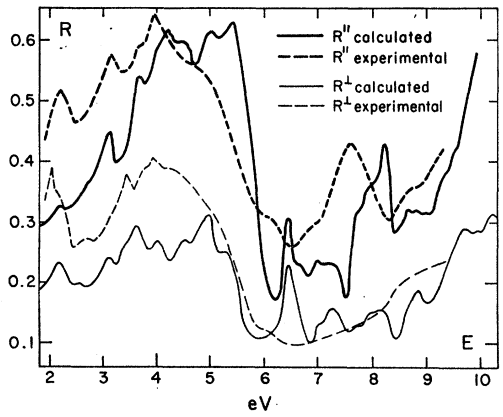

FIG. 12. Calculated and experimental reflectivity spectra.

[20] L. D. Landau and E. M. Lifshitz, *Electrodynamics of Continuous Media* (Pergamon Press, Inc., New York, 1960), pp. 260, 274.
[21] H. Gobrecht and A. Tausend, Z. Physik **161**, 205 (1961).

optical data for selenium by inspection of the energy bands alone has led to quite erroneous results,[2,8] especially since those bands were only known at a few symmetry points and axes. Early calculations[1,2] included merely the Δ axis and consequently tried to explain the reflectivity spectrum in terms of this single axis. However, Fig. 8 shows that this axis contributes very little, because the oscillator strengths are in general quite small.

Because the bands are flat, it was found that a decomposition of ϵ_2 into contributions from different bands rather than different regions in k space provides somewhat more understanding at least of the basic structure. Here the ultraviolet measurements of Mohler *et al.*[7] were most helpful as a test on our interpretation. More experimental work using modern differential techniques (piezoreflectance[22] or electroreflectance[23]) could, in the future, bring additional information about the location of certain transitions in the Brillouin zone—provided they are at all localized.

[22] U. Gerhardt, Phys. Status Solidi **11**, 801 (1965).
[23] B. O. Seraphin and N. Bottka, Phys. Rev. **145**, 628 (1966).

ACKNOWLEDGMENTS

This work was supported by the U. S. Army Research Office (Durham) and in part by the U. S. Atomic Energy Commission. I have further used facilities provided by the Advanced Research Projects Agency for materials research at the University of Chicago. The numerical calculations were carried out at the Computer Centers of the University of Chicago and the Argonne National Laboratory, whose services are appreciated. I wish to express my gratitude to Professor J. C. Phillips and Dr. Fred M. Mueller for numerous fruitful suggestions and advice. I have also benefitted from discussions with Professor M. H. Cohen, Professor David Brust, Dr. U. Gerhardt, and Dr. T. Bergstresser.

PHYSICAL REVIEW VOLUME 169, NUMBER 3 15 MAY 1968

Photoemission Study of the Electronic Structure of Wurtzite CdSe and CdS*

J. L. SHAY† AND W. E. SPICER
Stanford Electronics Laboratories, Stanford University, Stanford, California
(Received 5 October 1967)

In photoemission studies of single crystals of CdSe and CdS cleaved in vacuum, structure due to both direct transitions (**k** conserved) and nondirect transitions (**k** not important) is found. We explicitly separate the contributions to the energy distributions of the photoemitted electrons due to direct transitions from those due to nondirect transitions. By correlating structure in the energy distributions with structure in the reflectivity we determine (1) the energy of the initial and final states for the transitions causing this structure, and (2) the nature of the transitions (direct or nondirect or a combination of both). For CdSe we find that the transitions resulting in the E_2 reflectivity peak are direct and have initial states near -1.6 eV and final states near 5.8 eV (both with respect to the valence-band maximum). By comparing these initial and final states with the pseudopotential band structure of Bergstresser and Cohen, we find that these transitions occur at regions of the Brillouin zone around H and K. The E_1' reflectivity peak is due to direct transitions from initial states near -0.9 eV to final states near 7.5 eV; however, the region of the Brillouin zone involved is not certain. Whereas we show that the E_2 structure is almost entirely due to direct transitions, only about 20% of the absorption near the E_1' peak is due to direct transitions, the other 80% being due to nondirect transitions. We suggest that the F_3 reflectivity shoulder is due to nondirect transitions from a peak at -1.3 eV in the valence-band optical density of states to a peak at 7.5 eV in the conduction-band effective optical density of states. The nondirect transitions from this valence-band peak at -1.3 eV (and to this conduction-band peak at 7.5 eV) are observed over a wide range of photon energy. Direct transitions from initial states near the valence-band maximum are observed for $\hbar\omega \gtrsim 10.2$ eV. This suggests that there is a Γ conduction band near 10.2 eV. A deep valence band, tentatively identified as the cadmium 4*d* band, has been located at -9.9 eV. The results for CdS are similar, except that the relevant conduction-band states lie ~ 0.5 eV higher than in CdSe.

I. INTRODUCTION

THE purpose of this study has been to use photoemission techniques to investigate the electronic structure of wurtzite CdSe and CdS over a wide energy range. One of the principal advantages of the photoemission experiment is that it allows the determination of the absolute energies of the initial and final states for strong electronic transitions; conventional optical

* This work was supported by the National Aeronautics and Space Administration and the Advanced Research Projects Agency through the Center for Materials Research at Stanford and was based on a Ph.D. dissertation by J. L. Shay, Stanford University, 1966 (unpublished).
† Present address: Bell Telephone Laboratories, Holmdel, N. J.